

Inverted chemical force microscopy: following interfacial reactions on the nanometer scale

Barbara Dordi, Jason P. Pickering, Holger Schönherr, G. Julius Vancso *

Materials Science and Technology of Polymers, MESA⁺ Institute for Nanotechnology and Faculty of Science and Technology, University of Twente, 7500 AE Enschede, The Netherlands

Received 20 November 2003; received in revised form 9 January 2004; accepted 20 January 2004

Abstract

Atomic force microscopy (AFM) with chemical specificity using chemically modified AFM probes, so-called chemical force microscopy, was applied to study surface chemical reactions on the nanometer scale. To overcome the typical limitations of conventional AFM in following reactions in real-time, i.e. slow data acquisition, as well as thermal and instrumental drifts, we have introduced a new approach, named *inverted chemical force microscopy* (iCFM). In iCFM the reactants are immobilized on the AFM tip rather than on the substrate. The chemical reactions take place at the surface of the tip and are probed in real-time by force–displacement measurements on an inert octadecanethiol-covered Au substrate. The reactions studied were the hydrolysis and aminolysis of 11,11'-dithiobis(*N*-hydroxysuccinimidylundecanoate) (NHS-C₁₀). By iCFM intermolecular interactions and hence reaction kinetics can be quantitatively studied on the level of ~10–100 molecules. In particular, our iCFM data showed that the aminolysis reaction with *n*-butylamine on SAMs of NHS-C₁₀ is a spatially heterogeneous reaction. In addition, information about the defect density of reactive SAMs was obtained.

© 2004 Elsevier Ltd. All rights reserved.

Keywords: Atomic force microscopy; Reflection spectroscopy; Surface chemical reaction; Wetting; Gold; Biological molecules—nucleic acids; Biological molecules—proteins; Esters

1. Introduction

Self-assembled monolayers (SAMs) offer unique opportunities to increase the fundamental understanding of self-organization, structure–property relationships, and interfacial phenomena [1,2]. Their centrally important role as model systems for studies of physical chemistry and physics in two dimensions, respectively three dimensions [3], is based on their high level of structural definition, as well as their ease of access. SAMs provide the needed design flexibility, both at the individual molecular and at the material level, and offer

a vehicle for the investigation of specific interactions at interfaces, and in particular chemical reactivity of two-dimensional assemblies [4].

Chemical reactions on SAMs, as well as on other soft, i.e. organic or polymeric, surfaces play a crucial role in many applications, ranging from array technologies for genomics and proteomics [5] to (bio)sensors [6]. However, compared to reactions occurring in solution, chemical reactivity in ordered ultrathin organic films, such as Langmuir monolayers at the air–water interface [1,7] or SAMs on solid supports [1,8], can be very different. Since the functional groups or molecules involved in these reactions are packed more or less tightly at interfaces, these differences can be attributed to “confinement effects” [4,9]. Steric effects due to the necessary immobilization are likely to be exacerbated for certain surface reactions, leading to an energy barrier higher than would be expected in solution chemistry.

* Corresponding author. Tel.: +31-53-489-2974; fax: +31-53-489-3823.

E-mail address: g.j.vancso@utwente.nl (G. Julius Vancso).

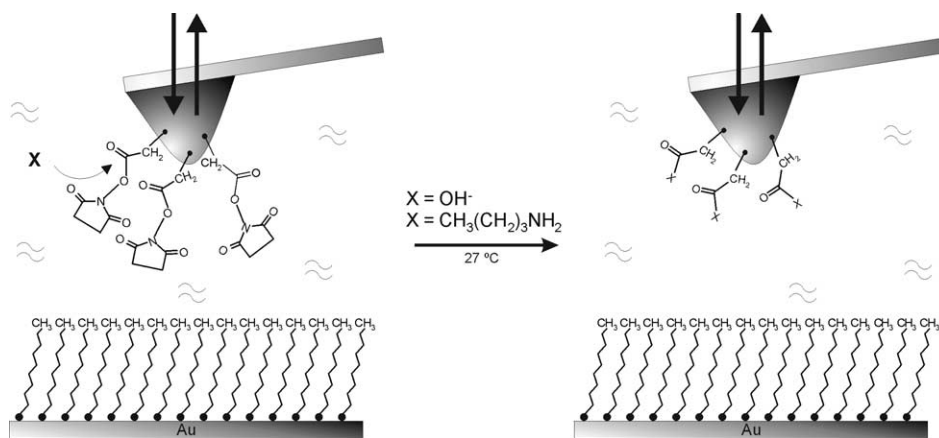


Fig. 1. Schematic of “inverted” chemical force microscopy for the reaction between NHS-esters and a nucleophile X. In this iCFM experiment, the pull-off forces between an AFM tip covered with a SAM of NHS-C₁₀ and an inert octadecanethiol SAM are measured in situ during the conversion of the reactive groups attached to the tip. The interaction between tip and inert surface varies with the extent of the reaction and hence allows one to quantitatively investigate the reaction kinetics on the nanometer level.

The rapidly continuing development of smaller bioarrays and protein chips with continuously increasing information density [10], as well as decreasing features sizes in, for instance, microfluidic devices and systems [11,12], impose more stringent requirements for the involved surface modification reactions [13]. Especially in the area of localized chemical reactions with sub-100 nm spatial control, new challenges in synthetic surface chemistry, as well as in the analysis of reactions at surfaces *at the relevant length scales*, must be addressed.

Using chemical force microscopy (atomic force microscopy (AFM) with chemical specificity) [14,15] local differences in chemical composition on a mesoscopic level and functional group distributions were determined in laterally resolved pull-off force [16–18] or friction force measurements. The approach relies on the measurement of intermolecular interactions between functional groups exposed on a chemically modified AFM tip with functional groups exposed on the substrate. Since the relation between pull-off force and the work of adhesion can be utilized to analyze changes in, e.g., surface free energy of the two contacting surfaces, spatial and temporal changes in chemical composition can be directly assessed [15]. Thus, surface reaction can be in principle followed by pull-off force mapping.

However, in addition to thermal and instrumental drifts, spatially *and* temporally resolved pull-off force measurements are limited by the currently very slow data acquisition [19]. These technical difficulties are eliminated in a novel approach, named “inverted” chemical force microscopy (iCFM) [20]. This approach was introduced to enable us to study surface reactions of organic thin films with nanometer-level adhesion measurements using AFM (Fig. 1).

In iCFM, the reactants are immobilized on the AFM tip rather than on the sample surface. The pull-off forces between the AFM tip covered with the reactant and an atomically smooth inert substrate are measured in situ during the reaction of the reactive groups with the other reactants that are dissolved in the imaging liquid. The interaction between tip and inert surface varies systematically with the extent of the reaction and hence allows one to quantitatively investigate the reaction kinetics. The compositional information obtained is confined to the contact area at pull-off, i.e. several nm² [15]. Therefore, interactions, local composition, and also reaction kinetics can be studied on the nanometer scale. As discussed here, this approach allows one to study and elucidate the origin of retarded or heterogeneously occurring surface organic chemical reactions on, e.g., granular gold surfaces at the relevant length scale.

In this paper we report on a systematic iCFM study of the kinetics and mechanisms of versatile reactions of an important class of bioreactive SAMs, namely SAMs of 11,11'-dithiobis(*N*-hydroxysuccinimidylundecanoate) (NHS-C₁₀) on Au.¹ The results reported here for the investigation of the base-catalyzed hydrolysis and aminolysis of NHS-C₁₀ show that this methodology is quantitative down to the molecular scale and is fully

¹ SAMs of NHS-C₁₀ have been used for the immobilization of native biomolecules onto gold, for the modification of gold surfaces with bioaffinity ligands, and for the development of gold biosensor chips (see, e.g. [21]). Previous work in our group has unveiled peculiar chain length-dependent reactivity differences of NHS-ester SAMs (Ref. [22]) indicating a reactivity decrease with improved packing (long chains).

applicable to a broad range of important solution phase (bio)organic surface reactions.

2. Experimental

2.1. Reagents

11,11'-Dithiobis(*N*-hydroxysuccinimidylundecanoate) (NHS-C₁₀) was synthesized as reported in Ref. [22]. *n*-Butylamine was obtained from Aldrich, sodium hydroxide concentrate (for preparation of volumetric solution 1.00×10^{-2} M) was obtained from Fluka. All the organic solvents, except for ethanol (p.a.; Merck), were purchased from Biosolve and used as received.

2.2. Contact angle measurements

The advancing and receding contact angles θ_{adv} and θ_{rec} , respectively, were measured with Millipore water as a probe liquid by using a contact angle microscope (Data Physics, OCA 15plus). Contact angles were determined at room temperature and ambient humidity. For this purpose a 1 μ l drop of water was placed on the monolayers. Water was then added to (removed from) the drop until the front was seen to advance (recede) across the surface. Once observable motion has ceased, the advancing (receding) contact angle was measured without removing the needle from the drop. A set of at least three different locations was averaged per monolayer sample.

2.3. Polarized grazing incidence reflection Fourier transform infrared (GIR-FTIR) spectroscopy

The FTIR spectroscopy data were collected using a BIO-RAD model FTS575C FTIR spectrometer using a GIR accessory (BIO-RAD) and a liquid nitrogen-cooled cryogenic mercury cadmium telluride (MCT) detector. Measurements were performed at room temperature; the spectrometer was continuously purged with nitrogen. The spectra were collected at an angle of incidence of 87° relative to the surface normal. 1024 scans recorded with a resolution of 4 cm⁻¹ were ratioed against the previously obtained background spectrum (SAM of *d*₃₃-hexadecanethiol on gold).

2.4. Kinetics studies

The hydrolysis and aminolysis of NHS ester SAMs were carried out in a thermostatted 1.00×10^{-2} M solution of NaOH and in a 3.00×10^{-2} M solution of *n*-butylamine, respectively. All experiments were carried out at 30 ± 0.5 °C (FTIR, CA) and 27 ± 2 °C (iCFM). Following the reactions, samples used for FTIR and CA measurements were rinsed with H₂O, 1 M HCl, H₂O, and finally with CHCl₃.

2.5. AFM tip modification

V-Shaped silicon nitride cantilevers with pyramidal tips (purchased from Digital Instruments, Santa Barbara, CA) were coated with ca. 2 nm of Ti and ca. 75 nm of Au by evaporation in high vacuum, followed by SAM deposition from 0.1 mM ethanolic solutions containing NHS-C₁₀ as described previously [18].

2.6. AFM measurements and analysis

The AFM measurements were carried out with a NanoScope III multimode AFM (DI) utilizing a 10 μ m (E) scanner and a DI liquid cell. The calibration of the AFM scanner in the *z*-direction was carried out using a set of three vertical calibration standards, TGZ 01-03, with step heights of 25, 104, and 515 nm, respectively (NT-MDT, Moscow, Russia). The cantilever spring constants (in the range of 0.05–0.12 N/m) were calibrated using the reference cantilever method described by Tortonese and Kirk [23] and by the thermal noise method [24]. The shape of the gold-modified tips was determined by imaging an array of sharp tips (TGT01, NT-MDT) and by scanning electron microscopy (JEOL JSM-T 220A).

2.7. Ester hydrolysis and aminolysis studied by iCFM

Force displacement data were acquired on a NanoScope III AFM (Digital Instrument, Santa Barbara, CA) with a custom-made signal acquisition setup and software analysis package. Using a signal breakout box (Signal Access Module, Digital Instruments, Santa Barbara, CA), the scaled voltage signals of the applied *z*-piezo position and the cantilever deflection signal were simultaneously measured with a data acquisition card (National Instruments, AT-MIO-16EX). Force curves (typically using a *z*-travel of 500–1000 nm) were acquired sequentially and analyzed in real time to determine the pull-off force, zero-deflection voltage, and maximum applied force. The pull-off force was measured for each force curve by determining the lowest cantilever deflection voltage value for each of the force curves and was logged to a data file before being analyzed further off-line. The mean values of each 200 sequentially captured pull-off events were calculated and plotted as a function of reaction time. For all pull-off force data we observed symmetric histograms.

3. Results and discussion

The reaction kinetics of the surface reactions described in this paper was first assessed on a “macroscopic” scale on substrates with self-assembled monolayers of NHS-C₁₀ (Fig. 2). During the reaction of the

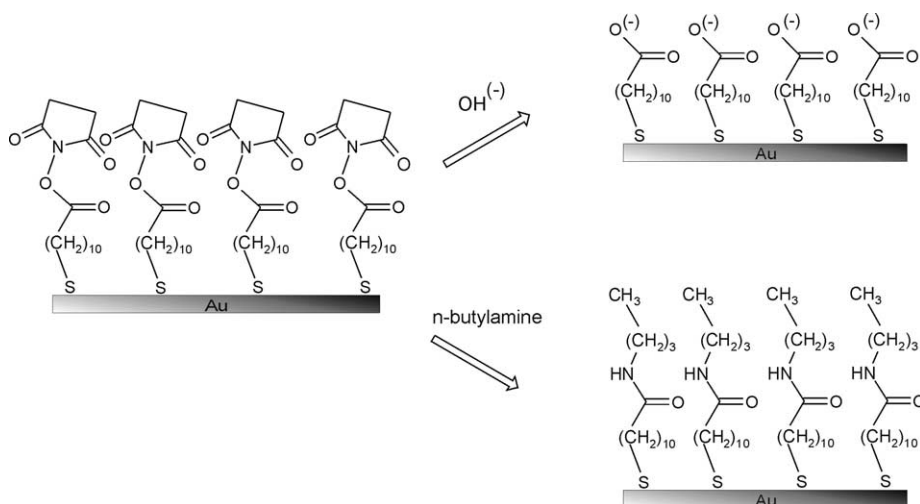


Fig. 2. Schematic illustration of the reaction between SAMs of NHS-C₁₀ and sodium hydroxide and *n*-butylamine, respectively.

SAMs of NHS-C₁₀ with sodium hydroxide (1.00×10^{-2} M) and *n*-butylamine (3.00×10^{-2} M) the corresponding carboxylate and amide-terminated SAMs were formed, as shown schematically in Fig. 2.

The progression of the hydrolysis and the aminolysis of the ester groups confined in the monolayers was determined by GIR-FTIR spectroscopy and contact angle measurements. In Fig. 3 the GIR-FTIR spectrum of NHS-C₁₀ adsorbed on gold is presented. During the reaction with 1.00×10^{-2} M NaOH at 30 °C the bands at ca. 2920 cm^{-1} and at ca. 2850 cm^{-1} , which are assigned to the asymmetric C–H stretching vibration, $\nu_{\text{as}}(\text{CH}_2)$, and to the symmetric C–H stretching vibration, $\nu_{\text{s}}(\text{CH}_2)$, respectively, do not show changes. The strong band at 1748 cm^{-1} , assigned to succinimidyl carbonyl, $\nu(\text{C}=\text{O})$, decreases in absorbance with the progress of the reaction and finally vanishes (Fig. 4c).

After the reaction of SAMs of NHS-C₁₀ with *n*-butylamine, the presence the amide I (1650 cm^{-1}) and amide II (1550 cm^{-1}) bands is diagnostic of the amide groups formed during the reaction (Fig. 4b). The disappearance of the succinimidyl ester bands is indicative of a complete consumption of the activated ester groups and thus a complete conversion.

For both reactions the kinetics was determined by measuring the decrease of the integrated intensity of the succinimidyl carbonyl band. The extent of the reaction x (Fig. 5) is expressed by

$$x = \frac{A_0 - A_t}{A_0 - A_\infty} \quad (1)$$

where A_0 is the integrated absorbance of the succinimide ester carbonyl band at time zero, A_t at time t , and A_∞ at infinitive time, respectively.

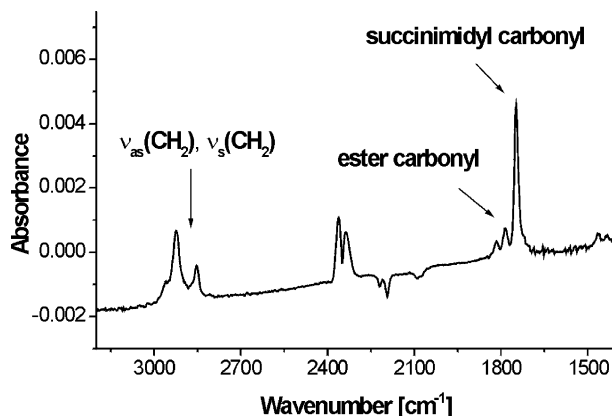


Fig. 3. GIR-FTIR spectrum of NHS-C₁₀ adsorbed on gold. The most prominent bands are the asymmetric C–H stretching vibration, $\nu_{\text{as}}(\text{CH}_2)$, at ca. 2922 cm^{-1} , the symmetric C–H stretching vibration, $\nu_{\text{s}}(\text{CH}_2)$, at ca. 2852 cm^{-1} , the C=O stretching vibrations, $\nu(\text{C}=\text{O})$, assigned to the ester carbonyl at 1815 and 1785 cm^{-1} , as well as to the succinimidyl carbonyl at ca. 1748 cm^{-1} .

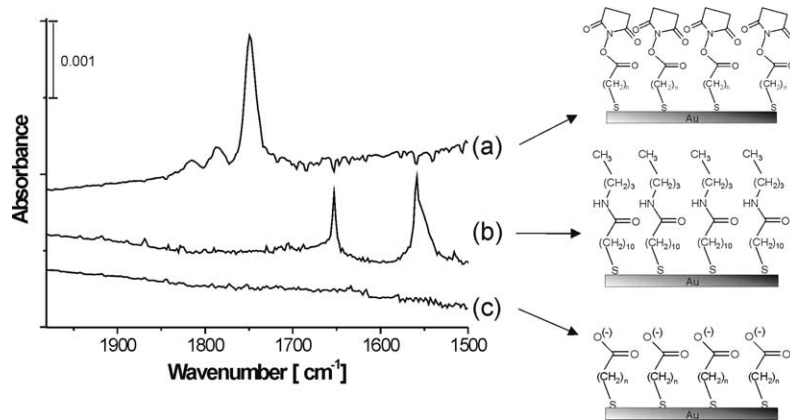


Fig. 4. Low-energy region of GIR-FTIR spectra of (a) NHS-C₁₀ adsorbed on gold, (b) NHS-C₁₀ on gold after reaction with 3.00×10^{-2} M *n*-butylamine at 30 °C, and (c) NHS-C₁₀ on gold after reaction with 1.00×10^{-2} M NaOH at 30 °C.

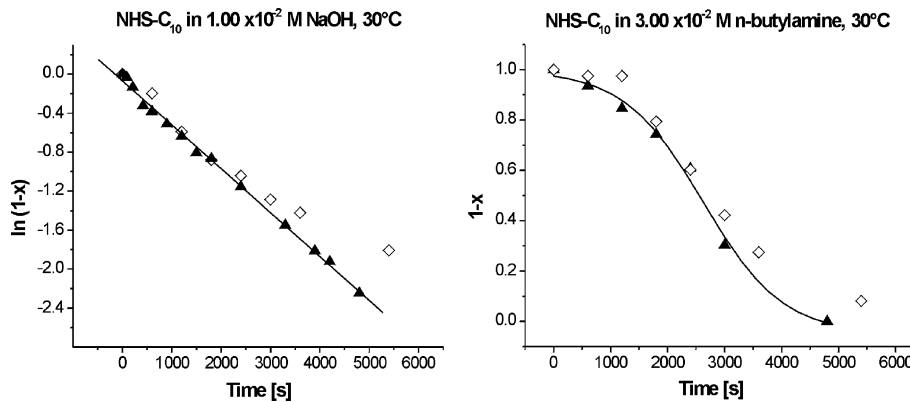


Fig. 5. Plots of $\ln[1-x]$ (x : extent of reaction) as function of reaction time for the hydrolysis (left) and plot of $[1-x]$ for the aminolysis of NHS-C₁₀ (right) as determined ex situ by FTIR spectroscopy (filled symbols) and by contact angle measurements (open symbols). The solid lines correspond to fits of the FTIR data (least-squares fit of the hydrolysis and sigmoidal fit for the aminolysis data, respectively).

The progression of the hydrolysis was also determined from the corresponding changes in contact angles (CA) as a function of time. Hydrolysis causes a significant increase in wettability with water, ($\theta_a(t=0) = 60^\circ$; $\theta_a(t=\infty) < 10^\circ$), while the aminolysis leads to an increase in hydrophobicity ($\theta_a(t=0) = 60^\circ$; $\theta_a(t=\infty) = 85^\circ$). If the two components in a mixed monolayer act independently and the effect of surface roughness and phase separation can be neglected, the experimentally determined contact angles θ_{exp} can be described by Cassie's equation. Therefore the surface coverage during the reactions was calculated by using Cassie's equation (Fig. 5) [25].

$$\cos \theta_{\text{exp}} = f_1 \cdot \cos \theta_1 + f_2 \cdot \cos \theta_2 \quad (2)$$

where f_1 and f_2 are the fraction of the surface having inherent contact angles θ_1 and θ_2 . For the quantitative

analysis of the CA data we restricted the analysis to conversions $< 40\%$ in order to avoid a correction of the CA data [28].

In the case of hydrolysis of SAMs of NHS-C₁₀ both FTIR and CA measurements showed an exponential decrease of NHS ester coverage with increasing reaction time. The calculation of the rate constants for the hydrolysis of NHS-C₁₀ was performed according to pseudo-first-order kinetics. The linearization of the FTIR spectroscopy data yielded a pseudo-first-order rate constant k' of $(4.5 \pm 0.4) \times 10^{-4} \text{ s}^{-1}$, the corresponding second-order rate constant k'' is $(4.5 \pm 0.4) \times 10^{-2} \text{ M}^{-1} \text{ s}^{-1}$, in agreement with contact angle data, which yielded a pseudo-first-order rate constant k' of $(4.5 \pm 2.3) \times 10^{-4} \text{ s}$.

In contrast to the hydrolysis, the aminolysis of NHS-C₁₀ showed a sigmoid kinetics with a half-life of the

reaction in 3×10^{-2} M aqueous *n*-butylamine of (2685 ± 40) s, in good agreement with the half-life of (2800 ± 40) s estimated from the CA data.

The FTIR and CA data suggest a homogeneously proceeding hydrolysis and a heterogeneously occurring aminolysis [4,20]. In order to confirm these hypotheses and to obtain a better understanding of these reactions we investigated the kinetics of the above-mentioned reactions on the relevant length scale, i.e. on the nanometer scale, by “inverted” chemical force microscopy (iCFM) (Fig. 1). In these experiments the force required to pull gold-coated AFM tips functionalized with SAMs of NHS-C₁₀ out of contact with an inert octadecanethiol SAM on flat Au(1 1 1) was monitored in real-time during the reaction in aqueous NaOH and *n*-butylamine for the hydrolysis and aminolysis, respectively.

The data were acquired with a frequency of one force–displacement curve per second and subsequently analyzed using a custom-made software. To calculate a mean pull-off force for a given time, 200 pull-off events were averaged. The changes in average pull-off forces are directly related to changes in surface composition of

the contact area at pull-off [14]. The corresponding pull-off forces were found to *decrease* for the hydrolysis (Fig. 6), while for the aminolysis the forces *increased* (Fig. 7). These trends are in full agreement with the expected trend in aqueous medium, where to a first approximation increasing hydrophobicity leads to increasing pull-off forces due to increasing solvent exclusion [26].

Fig. 6 shows clearly that during the hydrolysis the measured pull-off forces decreased right after the start of the experiment, while for the aminolysis an induction period (in Fig. 7, 1000–1500 s) was observed. In different iCFM experiments we recorded *vastly different* induction periods (vide infra).

From the measured changes in pull-off forces, the local composition and the conversion of the corresponding chemical reaction can be determined on the nanometer scale. The conversion x of ester groups to carboxyl or amide groups was calculated from

$$x = \frac{F_0 - F_t}{F_0 - F_\infty} \quad (3)$$

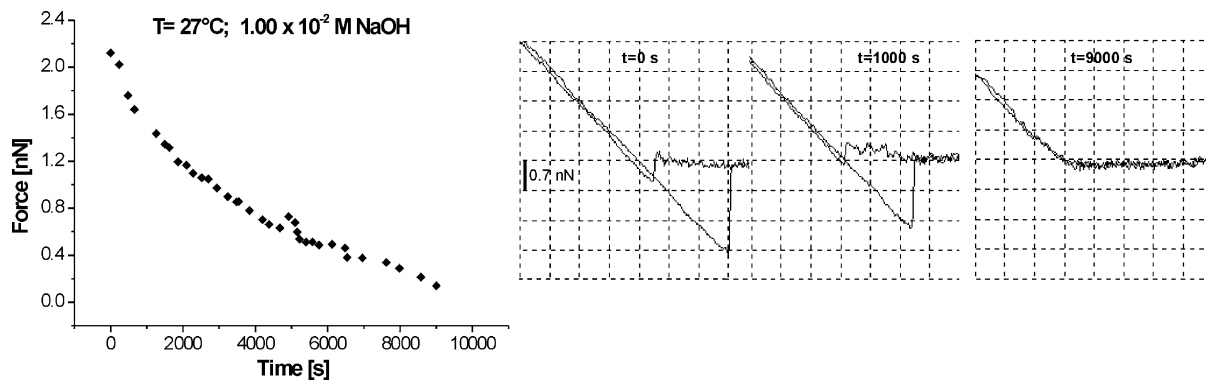


Fig. 6. Plot of pull-off forces as function of reaction time during hydrolysis of NHS-C₁₀ determined by iCFM, as well as representative force–displacement curves.

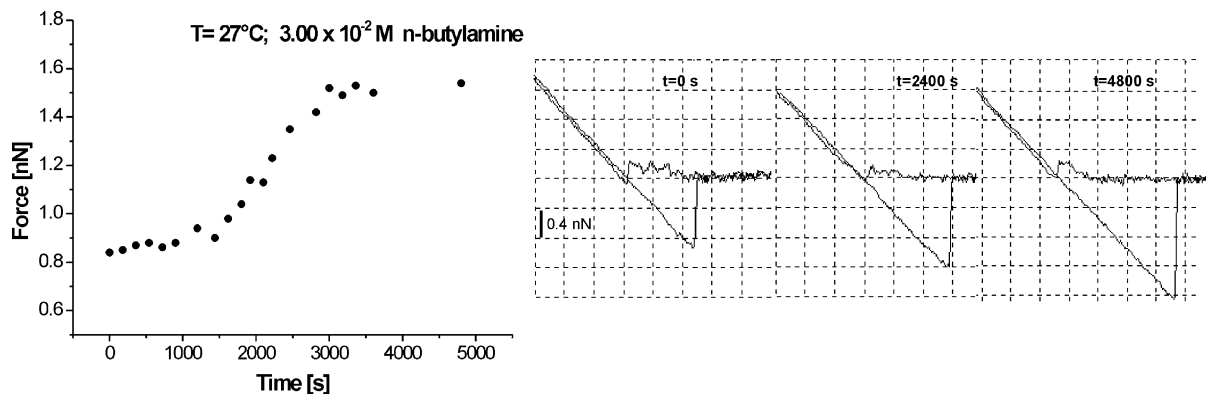


Fig. 7. Plot of pull-off forces as function of reaction time during hydrolysis (left) and aminolysis (right) of NHS-C₁₀ determined by iCFM, as well as representative force–displacement curves.

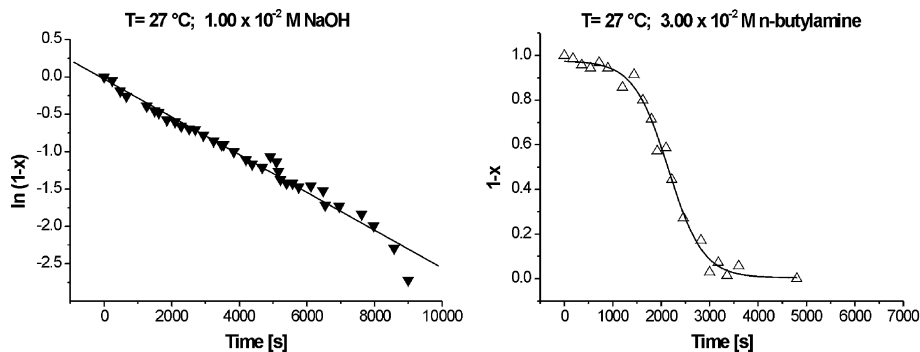


Fig. 8. Plots of $\ln[1 - x]$ (x : extent of reaction) as function of reaction time for the hydrolysis (left) and plot of $[1 - x]$ for the aminolysis of NHS- C_{10} (right) as determined in situ by iCFM. The solid line corresponds to a least-squares fit of the hydrolysis and a sigmoidal fit for the aminolysis data.

where F_0 , F_t , and F_∞ denote the measured average pull-off forces at $t = 0$, $t = t$, and $t = \infty$, respectively. This equation assumes that the forces change linearly with the work of adhesion [20,27]. The progress of the reaction is shown in Fig. 8.

The linearization of the surface coverages calculated from the iCFM data during the hydrolysis of NHS- C_{10} confirmed the previously observed pseudo-first-order kinetics for this reaction [22] and yielded a pseudo-first-order rate constant k' of $(3.0 \pm 0.3) \times 10^{-4} \text{ s}^{-1}$. This value is in good agreement with the FTIR data ($k' = (4.5 \pm 0.4) \times 10^{-4} \text{ s}^{-1}$) considering the slightly different reaction temperatures [28].

This result for the homogeneously occurring hydrolysis reaction shows in particular that the reaction can indeed be followed *quantitatively* on the scale of 20–50 molecules (*vide infra*) and that it proceeds on this scale similarly as it does on the scale of $>10^{12}$ molecules as sampled, e.g., by FTIR. Possible effects of the substrate roughness on local order are negligible,² since the type of gold surfaces is identical for the FTIR and iCFM measurements. In addition, pressure effects of the AFM tip that contacts the inert SAM periodically, diffusion and mixing problems of the reactants in solution, and limited stability of the SAMs in the reaction medium can be excluded. The data is also fully consistent with our previous report, where the reactivity of related ester-terminated SAMs was analyzed. In this case, high resolution AFM imaging before and after the reaction on Au(111) could be applied to verify the integrity of the SAM in molecularly resolved AFM images [20].

The aminolysis of NHS- C_{10} studied by iCFM shows a sigmoid kinetics with a mean half-life of the reaction in

$3.00 \times 10^{-2} \text{ M}$ aqueous *n*-butylamine of $(2600 \pm 10) \text{ s}$, which is in excellent agreement with the half-life of $(2685 \pm 40) \text{ s}$ estimated from the FTIR data. This mean value is the average of many individual experiments and shows that an average of the localized data indeed reproduces “macroscopic” kinetics quantitatively. On the other hand, each of the *individual* reaction profiles acquired on the nanometer scale contains novel nanometer scale information (Fig. 9).

In order to assess the sampling spot size, the number of interacting molecular pairs between the iCFM tips and SAMs of ODT on Au(111) was determined using the Johnson–Kendall–Roberts (JKR) theory of contact mechanics [30].³ An independent estimate was based on a statistical analysis of the observed rupture forces according to a method based on the analysis of the Poisson distribution [32]. We observe on average 20–50 interacting molecular pairs following both methods (Fig. 10). The spread in the numbers can be attributed to variations in tip radii, which is proportional to the pull-off force according to the JKR theory [31], and is likely determined by the grain size of the gold coating [20].

The very small contact area of 5–13 nm² was calculated from these numbers using an assumed area per molecule of 25 Å² [20,33,34]. The pseudo-first-order kinetics of the hydrolysis and the absence of any induction period indicate a spatially homogeneous reaction on the mentioned length scale. By contrast, the aminolysis is more interesting and reveals new information. In Fig. 10 a histogram of the induction periods observed for the aminolysis, as well as a plot of the

² Previous AFM work showed that the packing on granular gold is very similar to Au(111) [29a], although local disorder may be caused by granular gold resulting in altered average surface energies [29b].

³ Pull-off force measurements yielded the work of adhesion of $W_{12} = 11 \text{ mN/m}$ according to $F_{\text{pull-off}} = -3/2\pi R W_{12}$. The tip radius R was determined using scanning electron microscopy; the contact area at pull-off $A_{\text{pull-off}}$, using the JKR approach (Ref. [30]) was calculated as $A_{\text{pull-off}} = \pi(3\pi R^2 W_{12}/2K)^{2/3}$ where K denotes the reduced modulus ($K = 25 \text{ GPa}$, see e.g. [31]).

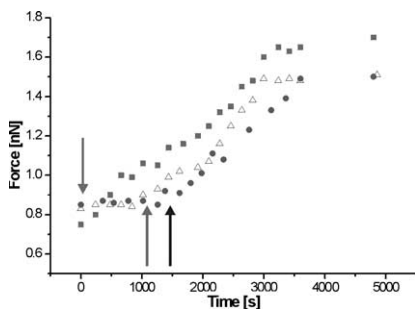


Fig. 9. Three individual aminolysis reactions followed by iCFM force measurements. The arrows indicate three widely different induction periods of ~ 0 , ~ 1000 , and ~ 1450 s.

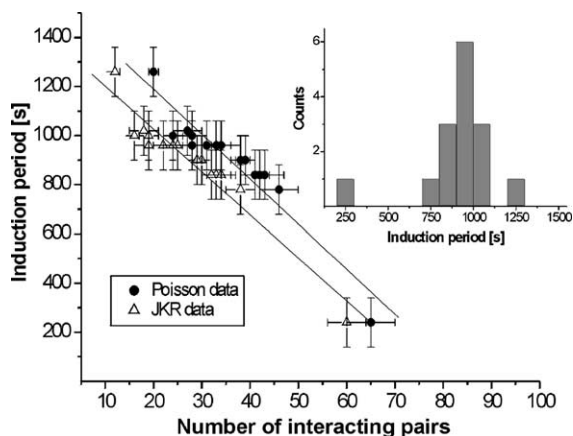


Fig. 10. Plot of induction period vs number of interacting pairs estimated using both the JKR theory and the Poisson method (inset: histogram of induction periods as measured by iCFM during aminolysis of NHS- C_{10}).

experimentally determined induction period vs the number of effectively interacting molecular pairs, are shown.

Based on a linear regression analysis, the average number of effectively interacting molecular pairs, for which the induction period becomes zero, is estimated to be 85 ± 4 pairs (Poisson) and 77 ± 3 pairs (JKR) (area ~ 20 nm²). Based on the interpretation that the reaction starts at defect or initiation sites, this value corresponds to 5×10^{11} defects/cm² and an approximate mean distance between neighboring defects of ~ 2.5 nm. By comparing these values with the number of pinholes found in etch-resistant SAMs of, e.g., ODT on gold (several thousand pinholes/cm²) [35], it seems that the initiation sites are unlikely pinholes, but may be defects in optimal head group packing [22].

Since we know that the change in surface free energy and hence work of adhesion and pull-off force is substantial for the studied reaction, any change in surface

composition of the molecules immobilized in the SAM on the tip must be accompanied by a change in pull-off force. Thus, the presence of an induction period indicates no significant conversion of the corresponding NHS ester groups. Thus, the occurrence of the induction periods for the aminolysis (Figs. 9 and 10) is a clear indication for the presence of a spatially heterogeneous reaction. Consequently, the distribution of the induction periods yields information on the monolayer structure and heterogeneity.

The heterogeneity can be caused by differences in packing in the SAM, such that the nucleophile experiences steric hindrance in more tightly packed areas of the SAM. Since *n*-butylamine is a bulkier and more hydrophobic nucleophile compared to the hydroxide ion, the heterogeneous reaction would be consequently only observed in the former case. Our experimental data thus indicate that the reaction may spread from initiation or defect sites that are initially accessible for nucleophilic attack. We speculate that at this very early stage, the reaction proceeds very slowly on average, as assessed by FTIR spectroscopy or contact angle measurements, because larger numbers of accessible reactive groups in the monolayer must first be generated as a consequence of the initial reaction. The reaction accelerates when more accessible reactive groups have been formed. As mentioned above, the observation of a broad range of induction periods is fully consistent with this model. If initiation or defect sites are present in or close to the small tip-sample contact area, the reaction can be detected at or just after the start of the experiment (Figs. 9, 10: $t_{\text{ind}} \leq 200$ s). In the case that the initiation or defect sites are located outside this contact area, the highly localized observation of the reaction only starts after the reaction has proceeded to the contact area (Figs. 7, 9, 10: $t_{\text{ind}} > 800$ s). Based on these data we can also estimate of the mean distance between the initiation or defect sites.

4. Conclusions

In this study we have shown that chemical reactions at interfaces can be quantitatively followed in situ on the level of as few as tens of molecules using inverted chemical force microscopy (iCFM). This methodology is fully applicable to a broad range of important solution phase surface reactions, such as those based on self-assembled monolayer coupling chemistry. For the aminolysis of NHS- C_{10} SAMs on gold, iCFM revealed in particular the progress of a spatially heterogeneous surface reaction on the nanometer scale. This observation is highly consistent with a reaction that proceeds by initiation at defect sites in the SAM. The mean distance between these defect sites was estimated as approximately 2.5 nm. These results, together with the quantitative information on kinetic parameters, such as rate

constants, show that iCFM may become a valuable tool to complement the development of optimized mesoscale and nanometer scale chemical arrays and functionalized devices.

Acknowledgements

This work has been financially supported by the Council for Chemical Sciences of The Netherlands Organization for Scientific Research (CW-NWO).

References

- [1] Ulman A. Introduction to thin organic films: from Langmuir–Blodgett to self-assembly. Boston: Academic Press; 1991.
- [2] (a) Nuzzo RG, Allara DL. *J Am Chem Soc* 1983;105:4481; (b) Schreiber F. *Prog Surf Sci* 2000;65:151; (c) Poirier GE. *Chem Rev* 1997;97:1117.
- [3] (a) Schmelmer U, Jordan R, Geyer W, Eck W, Golzhauser A, Grunze M, et al. *Angew Chem Int Ed* 2003;42:559; (b) Brower TL, Garno JC, Ulman A, Liu GY, Yan C, Golzhauser A, et al. *Langmuir* 2002;18:6207.
- [4] For a recent review on reactions and reactivity in SAMs, see: Chechik V, Crooks RM, Stirling CJM. *Adv Mater* 2000;12:1161.
- [5] (a) Lockhart DJ, Winzeler EA. *Nature* 2000;405:827; (b) Yee A, Pardee K, Christendat D, Savchenko A, Edwards AM, Arrowsmith CH. *Acc Chem Res* 2003;36:183; (c) Berhane BT, Limbach PA. *Anal Chem* 2003;75:1997.
- [6] Wang J, editor. *Biosensors and chemical sensors*. ACS Symp Ser 487. Washington, DC: ACS; 1992.
- [7] See e.g.: Roberts G, editor. *LB Films*. New York: Plenum Press; 1990.
- [8] Dubois LH, Nuzzo RG. *Ann Rev Phys Chem* 1992;43:437.
- [9] Ahmad J, Astin KB. *Langmuir* 1990;6:1797, and references therein.
- [10] (a) Niemeyer CM, Blohm DH. *Angew Chem Int Ed* 1999;38:2865; (b) Wang J. *Nucl Acids Res* 2000;28:3011; (c) Blohm DH, Guiseppi-Elie A. *Curr Opin Biotechnol* 2001;12:41.
- [11] (a) Sheehan AD, Quinn J, Daly S, Dillon P, O’Kennedy R. *Anal Lett* 2003;36:511; (b) Figeys D. *Proteomics* 2002;2:373.
- [12] (a) Beebe DJ, Mensing GA, Walker GM. *Ann Rev Biomed Eng* 2002;4:261; (b) Whitesides GM, Ostuni E, Takayama S, Jiang XY, Ingber DE. *Ann Rev Biomed Eng* 2001;3:335–73.
- [13] (a) Piner RD, Zhu J, Hong S, Mirkin CA. *Science* 1999;283:661; (b) Yang XM, Peters RD, Kim TK, Nealey PF, Brandow SL, Chen MS, et al. *Langmuir* 2001;17:228; (c) Li H-W, Muir BVO, Fichet G, Huck WTS. *Langmuir* 2003;19:1963.
- [14] Frisbie CD, Roznyai LF, Noy A, Wrighton MS, Lieber CM. *Science* 1994;265:2071.
- [15] For a review, see: Noy A, Vezenov DV, Lieber CM. *Ann Rev Mater Sci* 1997;27:381.
- [16] Weisenhorn AL, Maivald P, Butt H-J, Hansma PK. *Phys Rev B* 1992;45:11226.
- [17] Berger CEH, van der Werf KO, Kooyman RPH, de Grooth BG, Greve J. *Langmuir* 1995;11:4188.
- [18] (a) For functional group mapping in polymers, see e.g.: Schönherr H, Hruska Z, Vancso GJ. *Macromolecules* 2000;33:4532; (b) Schönherr H, van Os MT, Förch R, Timmons RB, Knoll W, Vancso GJ. *Chem Mater* 2000;12:3689.
- [19] van der Werf KO, Putman CAJ, de Grooth BG, Greve J. *Appl Phys Lett* 1994;65:1195.
- [20] Schönherr H, Chechik V, Stirling CJM, Vancso GJ. *J Am Chem Soc* 2000;122:3679.
- [21] Duhachek SD, Kenseth JR, Casale GP, Small GJ, Porter MD, Jankowiak R. *Anal Chem* 2000;72:3709.
- [22] Dordi B, Schönherr H, Vancso GJ. *Langmuir* 2003;19:5780.
- [23] Tortonese M, Kirk M. *Proc SPIE-Int Soc Opt Eng* 1997;3009:53.
- [24] (a) Hutter JL, Bechhoefer J. *Rev Sci Instrum* 1993;64:1868; (b) Sader JE. *Appl Phys* 1998;84:64.
- [25] Adamson AW, Gast AP. *Physical chemistry of surfaces*. 6th edition. New York: Wiley–Interscience; 1997. p. 355.
- [26] Sinniah SK, Steel AB, Miller CJ, Reutt-Robey JE. *J Am Chem Soc* 1996;118:8925.
- [27] Werts MPL, van der Vegte EW, Hadziioannou G. *Langmuir* 1997;13:4939.
- [28] Schönherr H, Feng C, Shovsky A. *Langmuir* 2003;19:10843.
- [29] (a) Schönherr H, Vancso GJ. *Langmuir* 1997;13:3769; (b) Yang J, Han J, Isaacson K, Kwok DY. *Langmuir* 2003;19:9231.
- [30] Johnson KL, Kendall K, Roberts AD. *Proc R Soc London A* 1971;324:301.
- [31] Skulason H, Frisbie CD. *Anal Chem* 2002;74:3096.
- [32] Stevens F, Lo Y-S, Harris JM, Beebe Jr TP. *Langmuir* 1999;15:207, and references cited therein.
- [33] Nelles G, Schönherr H, Jaschke M, Wolf H, Schaub M, Küther J, et al. *Langmuir* 1998;14:808.
- [34] Schönherr H, Vancso GJ, Huisman B-H, van Veggel FCJM, Reinhoudt DN. *Langmuir* 1999;15:5541.
- [35] Wilbur JL, Whitesides GM. In: Timp G, editor. *Nanotechnology*. New York: Springer; 1999. p. 339.